We are IntechOpen,
the world's leading publisher of
Open Access books
Built by scientists, for scientists

6,900
Open access books available

186,000
International authors and editors

200M
Downloads

154
Countries delivered to

Our authors are among the

TOP 1%
most cited scientists

12.2%
Contributors from top 500 universities

WEB OF SCIENCE™

Selection of our books indexed in the Book Citation Index
in Web of Science™ Core Collection (BKCI)

Interested in publishing with us?
Contact book.department@intechopen.com

Numbers displayed above are based on latest data collected.
For more information visit www.intechopen.com

Photoelastic Modulated Imaging Ellipsometry

Chien-Yuan Han, Yu-Faye Chao and Hsiu-Ming Tsai

Additional information is available at the end of the chapter

Abstract

Photoelastic modulator (PEM)-based ellipsometry employed either lock-in amplifiers or the Fourier analysis technique to obtain the ellipsometric parameters almost in real-time that makes the system with a feature of fast measurement speed, higher stability, and sensitivity at small retardations. Since the PEM modulation frequency is too high to compare it with the exposure time of the camera, photoelastic modulator–based approach is not applicable for a two-dimensional ellipsometric measurement. Here, we represent a novel technique that coordinates with the light pulses and PEM modulation that can freeze the time-varied signals. Thus, two-dimensional ellipsometric parameters can be obtained within few seconds. In addition to ellipsometric measurement, this approach also can be extended to other imaging polarimetry measurements, such as Stokes parameters and Mueller matrix. Moreover, since the chromatic dispersion of birefringence was also a significant issue in the polarization modulation systems, we proposed an equivalent phase retardation technique to deal with this issue. This technique was confirmed by a dual wavelength measurement result without changing the optical configuration of the system. The concept and the theory of this system were indicated in the preceding section, and the passage below described some calibration issues for the photoelastic modulator. Some measurement results were revealed in the final part of this chapter.

Keywords: photoelastic modulator, imaging polarimetry, ellipsometric parameters, Stokes parameter, Mueller matrix, dual wavelength

1. Introduction

Among other optical techniques, ellipsometry is one of the most powerful tools for characterizing optical properties, including determining film thicknesses and refractive indices with a high degree of accuracy. Currently, common applications of ellipsometry include measuring thin films for solar cells, optical coatings, microelectronics, and biosensing applications [1–3]. However, most ellipsometric measurements are based on a single point and use a

single-wavelength or spectroscopic approach [4, 5]. As the size of many electronic devices becomes smaller, the uniformity of the thin-film thickness, a high degree of resolution, and a large field of view become more desirable for industrial applications. Therefore, ellipsometry with a spatially resolved capability to assess two-dimensional morphologies of a surface is a natural evolution of ellipsometric measurement techniques that extend the single spot ellipsometric measurement to a tool to visualize and analyze microscopic images for thin films [6, 7]. Thus far, the commercial imaging ellipsometer usually operated on the principle of the classical null technique; instruments used are typically equipped with stepping motors to change the azimuth angle of the polarizer, compensator, or analyzer; and they use charge-coupled device (CCD) or complementary metal-oxide-semiconductor (CMOS) detectors to take a sequence of images in order to gather enough information to calculate all null positions [6]. This approach is relatively slow and is limited by the mechanical rotation speed, and the modulation frequency usually falls within a noise range of other mechanical devices; this impedes data acquisition and, eventually, system stability. In addition, for a sample with inhomogeneous surface characteristics, the measurement process may need to collect many more images to determine the null positions of each measurement point; this makes the measurements relatively cumbersome and impractical for industrial applications.

Another popular approach for imaging ellipsometry was using photometric measurement technique, which few intensity images captured at various angles of polarization elements to deduce ellipsometric distributions of the sample [8–10]. However, this approach requires the rotation of polarization elements and suffers the issue of beam wander during the rotation, possibly resulting in mismatching the interest point in a sample and a recording pixel associated with different images. The above issues make the measurement troublesome especially for spatially nonuniform objects or imperfectly uniform incident beam. Compared with null ellipsometry, photometric ellipsometry is faster, and the measurement quality is improved. Phase modulated apparatus is also involved in the ellipsometric measurement. The ellipsometer based on the use of a photoelastic modulator (PEM) is the most prevalent configuration; it has a typical modulation frequency of 50 kHz with no moving parts [11–13]. For single spot measurement, one can employ either lock-in amplifiers or the Fourier analysis technique to obtain the ellipsometric parameters in near real-time, but this approach is not applicable for a two-dimensional measurement, because the modulation frequency of the PEM is too high to compare it with the exposure times of the CCD camera. This deficiency was overcome by replacing the light source with an ultra-stable short pulse, known as the stroboscopic illumination technique, which was synchronized with the PEM modulation to freeze the intensity signal at specific times in the modulation cycles [14, 15]. As a result, the ellipsometric images can be obtained in seconds by sequentially taking four images with single wavelength source. Since Stokes parameters were related to the ellipsometric parameters by their definitions, Stokes parameters also can be measured through the use of the same approach [16]. In order to remove the chromatism limits of this system, we adopted an equivalent phase retardation technique that used dual wavelength ellipsometric measurement to extend the imaging ellipsometry technique without any adjustment of the photoelastic modulator or the optical configuration. Moreover, the image acquisition time for one set of ellipsometric parameters for

dual-wavelength measurement remained virtually unchanged [17]. This technique was also applied in Mueller matrix imaging system; we introduced a hybrid phase modulation technique to evaluate the optical polarization characteristics of the specimens [18]. In this chapter, we introduced the principle of the system, explained how this concept can be used in imaging ellipsometric measurement, and demonstrated dynamic measurement results. As PEM is the crucial component in this system, some calibration processes are also discussed in this chapter.

2. Theory and optical configuration of the photoelastic modulated imaging ellipsometry

Ellipsometry measures the changes of a polarized light that is reflected from the sample surface; such changes can be used to deduce the optical parameters of the sample. The ellipsometric parameters, Ψ and Δ, are defined as:

$$\tan \Psi e^{i\Delta} = \frac{r_p}{r_s} \tag{1}$$

where r_p and r_s are the complex Fresnel reflection coefficients for polarized light that is parallel and perpendicular to the plane of incidence, respectively [4]. The compensator was replaced by a PEM in the polarizer-compensator-sample-analyzer setup, as shown in **Figure 1**. The output polarization state can be represented by the operation of their corresponding Mueller matrices; i.e., the polarization state can be expressed as:
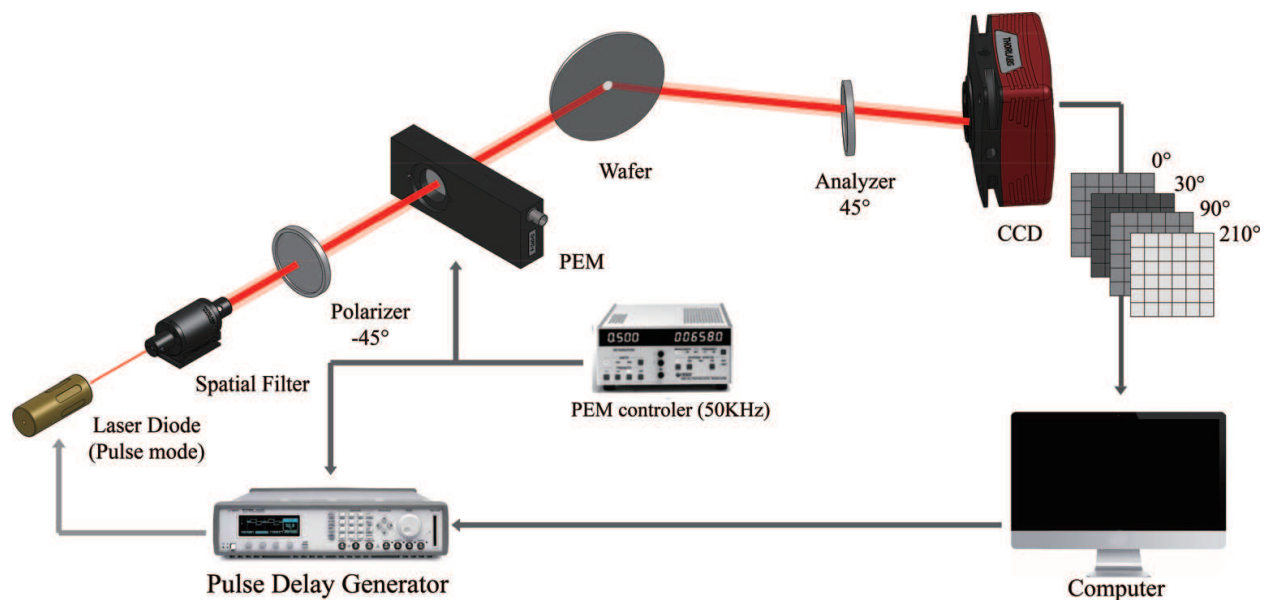

Figure 1. Experimental setup of the photoelastic modulated imaging ellipsometry by stroboscopic illumination technique.

$$S_f = M_A(A) \cdot R_{SAM}(\Psi, \Delta) \cdot M_{PEM}(\theta, \Delta_P) \cdot S_P \tag{2}$$

where S_f and S_P are Stokes vectors of the output polarization state and the incident linearly polarized light at the azimuth angle of P, respectively. Moreover, $M_{PEM}(\theta, \Delta_P)$, $R_{SAM}(\Psi, \Delta)$, and $M_A(A)$ represent the Mueller matrix of the PEM, the sample, and the analyzer, respectively. In this configuration, the optic axis of the PEM is at 0° with respect to the incident plane. When P = −45° and A = 45°, the reflected intensity can be found to be:

$$I(t) = \frac{I_0}{2}[1 + \sin 2\Psi \cos(\Delta - \Delta_P) \tag{3}$$

where I_0 is the normalized output intensity, and Δ_P is the phase retardation of the PEM, which is modulated as $\delta_0 \sin \omega t$. If one set of the amplitude of modulation δ_0 equals π, the temporal intensity behavior can be formulated as:

$$I(t) = \frac{I_0}{2}[1 + \sin 2\Psi \cos(\Delta - \pi \sin \omega t)] \tag{4}$$

When the temporal phase angles ωt in Eq. (4) are 0 and 90°, the corresponding intensities can be expressed as:

$$I_{0°} = \frac{I_0}{2}[1 + \sin 2\Psi \cos \Delta] \tag{5}$$

and

$$I_{90°} = \frac{I_0}{2}[1 - \sin 2\Psi \cos \Delta] \tag{6}$$

respectively. It is easy to prove that:

$$\sin 2\Psi \cos \Delta = \frac{I_{0°} - I_{90°}}{I_{0°} + I_{90°}} = I' \tag{7}$$

Using the similar process for ωt at 30 and 210°, one can obtain:

$$\sin 2\Psi \sin \Delta = \frac{I_{30°} - I_{210°}}{I_{30°} + I_{210°}} = I'' \tag{8}$$

Thus, the ellipsometric parameters can be obtained by measuring the intensity at above four temporal phases, as follows:

$$\Delta = \tan^{-1}\left(\frac{I''}{I'}\right) \tag{9}$$

$$\Psi = \frac{1}{2}\sin^{-1}\left(\sqrt{I'^2 + I''^2}\right) \tag{10}$$

The time-varying signal can be frozen at these temporal phases by illuminating the objects with short synchronized light pulses.

2.1. Interpretation of stroboscopic illumination applied in PEM imaging system

For a conventional phase modulated ellipsometer, photoelastic modulator is the most prevalent modulator installed in the ellipsometric system. The photoelastic modulator oscillates at its resonance frequency (typically around 50 kHz), and the response time of the phase modulated ellipsometer can reach as short as 1 ms/point to achieve the requirement for real-time monitoring and dynamic studies [19–21]. Although the ellipsometer using photoelastic modulator to modulate or examine polarization states has the advantages of being very fast, having no moving elements for acquiring signals, the high frequency of modulation was also an issue for the two-dimensional measurement due to the fact that the modulation frequency is much higher than the image sensor frame rate. To overcome this issue, two approaches are developed in recent days. One approach was using two or four PEMs and field-programmable gate array (FPGA)-assisted sequential time gating approach. In that configuration, four PEMs are set at different azimuths, and their modulation frequencies also have to be different from each other. The frequency drift of PEMs and image recovery were taken more effort on calibration and measurement [22–25]. We adopted a simple approach by just changing the manner of light illumination from continuous mode to pulse mode, which coordinates with the reference signal of the PEM modulator, known as the stroboscopic illumination technique [14–18]. Stroboscopic effect is a result of temporal aliasing that occurs when continuous motion is represented by a series of short samples. If the motion is circular or repeating, such as a spinning wheel or a vibrating membrane, and the frequency of light pulses and wheel speed or membrane oscillation are the same, the wheel or the membrane will appear stopped. In our system, PEM modulator functioned as a resonant device and operated at a fixed frequency about 50 kHz; therefore, while the light pulses coordinate with the resonant frequency of the PEM, the phase retardation of the modulator can be fixed at a specific value, rather than a continuous variation as a function of time. The synchronization process between the light pulses and PEM modulator was through the square wave reference signal, as the extra-trigger, of the PEM controller to initiate light pulses whose width was 110 nm (~2° phase change of modulator) from diode lasers. Another issue to be considered was how to shift the phase of the modulated optical signal that can generate different polarizations of the outgoing light. This feature can be achieved by the digital delay function of the pulse generator that provides defined pulses at four specific intervals, which are 0, 30, 90, and 210°, as shown in **Figure 2**. The $\omega t = 0°$ pulse, the beginning of a modulation cycle, is generated by the pulse generator, and then the time shift delays of the pulses are sequentially set on the basis of temporal phase angle ωt, i.e. 30, 90, and 210°, of the PEM modulation. After setting the light pulses at the proper triggering and delay outputs, the output polarizations can appear to be frozen by use of the stroboscopic illumination technique. For the image acquisition, the exposure time Δt of the CCD camera was at the range of decisecond to several seconds depending on the intensity of the diode laser and the sensitivity of the camera. For maintaining the intensity in the linear range, four specific images at different temporal phase angles were obtained to deduce the two-dimensional ellipsometric parameters.
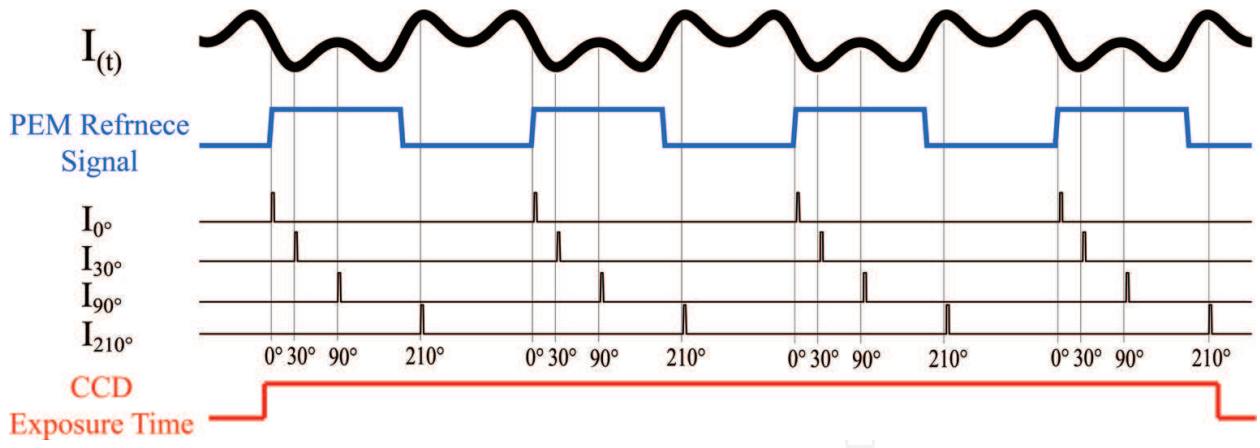
Figure 2. The principle of image acquisition: each intensity ($I_{0°}$, $I_{30°}$, $I_{90°}$, $I_{210°}$) was obtained by the accumulation of N short pulses of the modulated signal I(t) at a specific temporal phase angle at the fixed exposure time of the camera. The four intensities were acquired in sequence by the synchronized ultrastable short-pulse illumination. The ellipsometric images are calculated by these four intensities.

2.2. Issues in calibration of the PEM imaging system

All ellipsometric methods require azimuthal alignment of the polarizers, retarders, and phase modulators, with respect to the plane of incidence. If this alignment is not accurate, the systematic error appears in the ellipsometric measurements. Overlooking the azimuthal align‐ment of the polarizer and analyzer, there are some alignment issues that have to be addressed in a PEM-based ellipsometer and that are discussed below:

2.2.1. Azimuth angle calibration of the photoelastic modulator

It is essential to align the azimuths of the optical components in the ellipsometer for accurate measurement because any improper azimuth setting in the system can cause significant errors. The null method, locating the minimum intensity, is a typical azimuthal alignment technique in most ellipsometric systems. Since the minimum intensity must be determined precisely in the null method, a highly sensitive detection apparatus is required in those techniques. Instead of using the null method, we proposed an intensity ratio technique and separately aligned the azimuths of the polarizer and analyzer to the specimen surface in a polarizer-sample-analyzer (PSA) system [26, 27]. After precisely locating the incident plane in the PSA system, we then shift the attention to determine the strain axis of PEM to the incident plane. If the strain axis of PEM deviates from the incident plane by θ, and the impinging light is a +45° linear polarized light, the intensity can be reformulated from Eq. (5) as:

$$I_{(A)} = I_0 \left[L \sin^2 A + M \cos^2 A \tan^2 \Psi + N \sin A \cos A \right] \tag{11}$$

where

$$L = \frac{1}{2}[1 + \cos \Delta_P + (1 - \cos \Delta_P)(1 - \sin 4\theta)]$$

$$M = \frac{1}{2}[1 + \cos \Delta_P + (1 - \cos \Delta_P)(1 + \sin 4\theta)]$$

$$N = \frac{1}{2}[1 + \cos \Delta_P - (1 - \cos \Delta_P) \cos 4\theta] \tan \Psi \cos \Delta - \sin \Delta_P \cos 2\theta \tan \Psi \sin \Delta$$

When the A = 0 and 90°, the expression of intensity can be reduced and expressed as:

$$I_{(0°)} = \frac{I_0}{2} \tan^2 \Psi [2 + (1 - \cos \Delta_P) \sin 4\theta] \tag{12}$$

$$I_{(90°)} = \frac{I_0}{2} [2 - (1 - \cos \Delta_P) \sin 4\theta] \tag{13}$$

If the phase modulation Δ_P is modulated as $\delta_0 \cos \omega t$, then the intensity can be Fourier expanded by its harmonic function:

$$\cos \Delta_P = J_o(\delta_o) - 2J_2(\delta_o) \cos 2\omega t \tag{14}$$

By taking the zero-order Bessel function $J_0(\delta_0)$ at its zero point, i.e., $\delta_0 = 0.383\lambda$, we can simplify the DC component of its intensity as:

$$I_{(0°)} = \frac{I_0}{2} \tan^2 \Psi [2 + \sin 4\theta] \tag{15}$$

$$I_{(90°)} = \frac{I_0}{2} [2 - \sin 4\theta] \tag{16}$$

From Eqs. (14) and (15), the azimuth deviation of the PEM can be obtained by the DC component of the intensity, which is taken at two azimuths of the PEM separated by 45° through the following relation:

$$\sin 4\theta_o = 2 \frac{I_{dc}(0°)_{\theta=\theta_0} - I_{dc}(0°)_{\theta=\theta_0+45°}}{I_{dc}(0°)_{\theta=\theta_0} + I_{dc}(0°)_{\theta=\theta_0+45°}} \tag{17}$$

In addition to the azimuth determination, the ellipsometric parameter Ψ can also be obtained by the same measurements as:

$$\tan^2 \Psi = \frac{I_{dc}(0°)_{\theta=\theta_o+45°}}{I_{dc}(90°)_{\theta=\theta_o}} \tag{18}$$

Eq. (16) is sufficiently general to analyze the error of the azimuth deviation. According to the intensity ratio of Eq. (16), one can easily prove that the deviation of azimuth $\delta\theta_0$ caused by those fluctuations is:

$$\delta\theta_o = \frac{\tan 4\theta_0}{4 \tan^2 \Psi} \frac{\delta I}{I} \tag{19}$$

2.2.2. Amplitude modulation calibration of the photoelastic modulator

Even if all the azimuths of the optical components can be aligned in a PEM ellipsometer at a fixed incident angle, the modulation amplitude of PEM still needs to be calibrated. The conventional technique for calibrating the modulation amplitude is to adjust the oscilloscope waveform of a half-wave modulation in a straightforward setup, and a multiple-paths method is used to amplify the modulation amplitude for higher resolution. However, this technique was not proceeded under reflection configuration and did not meet the requirement of in-situ

calibration of the ellipsometer. We introduce a technique for the calibration of the modulation amplitude of PEM by a multiple harmonic intensity ratio (MHIR) technique whose setup was the same as for the ellipsometric measurement [28]. As a result, the modulation amplitudes of the PEM can be determined by using the intensity ratios of I_{1f}/I_{3f} (odd ratio) and I_{2f}/I_{4f} (even ratio) by the following:

$$\frac{I_{1f}}{I_{3f}} = \frac{J_1(\delta_0)}{J_3(\delta_0)}; \frac{I_{2f}}{I_{4f}} = \frac{J_2(\delta_0)}{J_4(\delta_0)} \tag{20}$$

It is clear that these ratios are independent of the azimuth position of the analyzer and the physical parameters of the examined sample. In this way, the optical characteristics of the PEM can be completely recognized.

2.2.3. Initial phase determination of the photoelastic modulator

Compared with the conventional continuous wave modulation, our approach employed the pulse lights initiated at different phase angles. Therefore, the additional condition, initial phase angle of the pulse light, has to be checked before the measurement. In the previous section, we demonstrated that four temporal phase angles ωt, 0, 30, 90, and 210°, were set to initiate pulse lights, triggered by the external square wave, from the PEM controller. However, we found reference zero of the square wave does not match with the initial phase of optical modulation signal, as shown in **Figure 3**, which means further determination of the phase shift of both signals is required. The determination process was carried out by an additional intensity
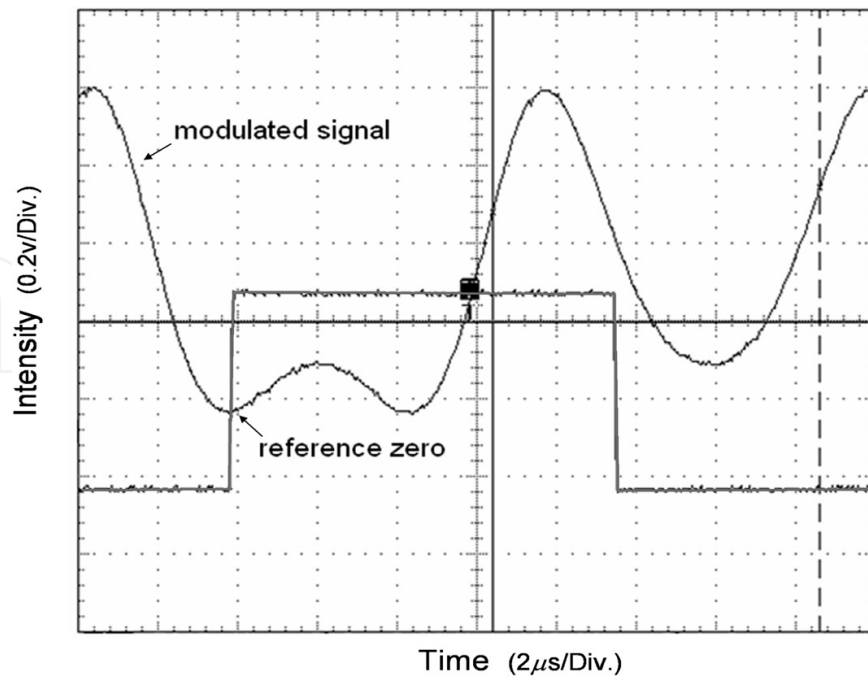

Figure 3. The temporal waveform of the Pt/Si thin film and the reference square wave provided by the PEM; the local minimum intensity does match with the reference zero.

measurement at $\omega t = 180°$. If the phase shift between the square reference signal and modulated optical signal is x, one can determine x by the following equation:

$$\frac{I_{210°} - I_{30°}}{I_{180°} - I_{0°}} = \frac{\sin\left(\pi \sin(x)\right)}{\sin\left(\pi \sin\left(x + \pi/6\right)\right)} \tag{21}$$

This ratio can eliminate the effect of ellipsometric parameters and normalized intensity, so it is free from the material under investigation. As a result, the phase shift can be solved by the intensity measurements at $\omega t = 0, 30, 180,$ and $210°$ according to Eq. (20). The correction of phase shift x can also be achieved by the time shift delays of the pulses [15].

3. Two-dimensional measurement results for ellipsometric parameters, Stokes parameters, and Mueller matrix

3.1. PEM imaging system for the static ellipsometric measurement

An L-shaped SiO_2 layer with the thickness of 50 nm on a silicon substrate was set as the static sample to examine the feasibility of the stroboscopic illumination imaging ellipsometry. Before the examination, the light beam was expanded to cover the whole L-shaped pattern, and the deduced thickness profile is shown in **Figure 4**. One can observe the plateau of the thickness profile was about 52 nm, which was consistent with the thickness before etching. The inset of **Figure 4** shows the valley of the profile is 2 nm oxide layer after the etching process, and this result was ignored at the 2° static phase retardation of PEM.

3.2. PEM imaging system for a dynamic ellipsometric measurement

Besides the static measurement, an oil droplet movement sliding on the surface of a vertical bare silicon wafer was regarded as the dynamic test for this imaging ellipsometric measurement system. This work was carried out at the incident angle of 70°, and 2 μl oil droplet
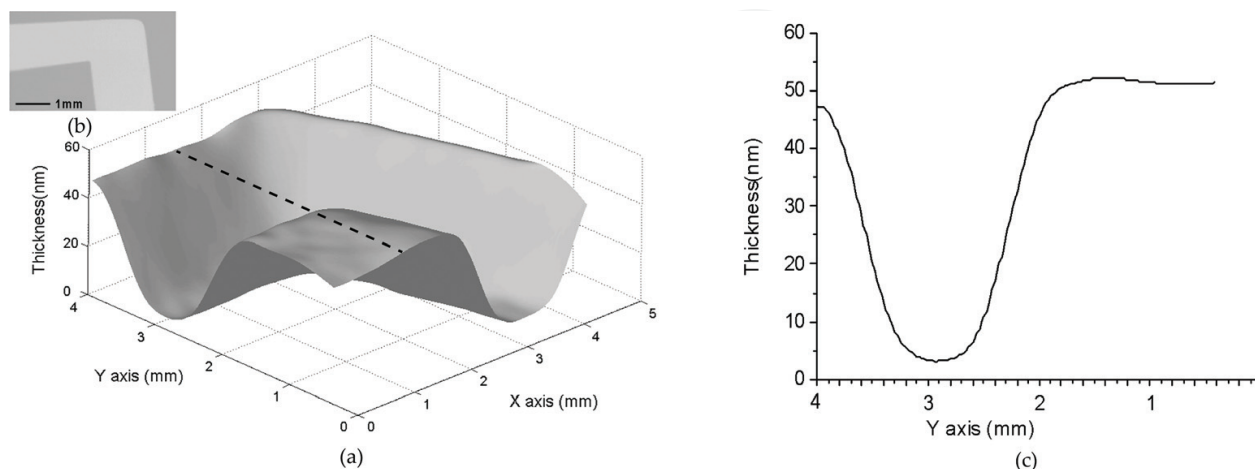

Figure 4. The L-shaped SiO_2 layer: (a) the two-dimensional thickness profile, (b) the photo image, and (c) the thickness profile of the SiO_2 film at x = 1.5 mm.

(Nikon, nd = 1.515) with high viscosity flowed slowly from the top of the vertically held silicon wafer. The total acquisition time of one set of ellipsometric parameters is about several tens of seconds, depending on the frame transfer speed of the camera. **Figure 5** demonstrates six sets of ellipsometric parameters during the oil dropping process.

3.3. Optimization for PEM Stokes imaging system

The Stokes parameters can be represented in the ellipsometric parameters by their definitions, as shown in **Figure 6**. If the input light is the +45° linear polarized light, the normalized output (reflected or transmitted) Stokes vector S = [S_0 S_1 S_2 S_3] can be expressed in the form of ellipsometric parameters as S = [1 cos(2Ψ) sin(2Ψ)cos(Δ) sin(2Ψ)sin(Δ)] [29]. Using the linear transformation model of polarimetry, we can write {b} = [A] {s}, where {b} is an N-element vector of the measured irradiances; [A] is an N × 4 matrix, the measurement matrix [30]; and {s} is the Stokes vector. Since {s} = [A]$^{-1}$ {b}, each element represents the response of the unit stimuli of the system. The noise in the measurement of the Stokes vector can be expressed in a vector form {n}; therefore, the error {ε} can be expressed as {ε} = [A]$^{-1}$ {n}. Since all components of the Stokes vector are weighted in noise production equally, the equally weighted variance (EWV) [29] figure of merit for N measurements can be expressed as follows:

$$EWV = \sum_{j=0}^{3} \sum_{k=0}^{N-1} \left([A]^{-1} \right)_{j,k}^2 = Tr\left[[A]^{-1} \left([A]^{-1} \right)^T \right]. \tag{22}$$

This value demonstrates the measurement errors by summing all entries in the measurement matrix. The polarization state analysis portion of the PEM polarimetry consists of a photoelastic modulator and an analyser, whose azimuth angles were set at 0 and 45°, respectively. The kth row of the matrix [A]$^{-1}$ of the phase lock configuration can be expressed as [1 0 cos(Δ_P) sin(Δ_P)]^T, where $\Delta_P = \delta_0 \sin\omega t$ is the phase retardation of the PEM. By taking the modulation amplitude to be half-wave (i.e., $\delta_o = \pi$), one can set the temporal phase at $\theta = \omega t$ instead of moving the conventional rotating angles θ in space.

In this PEM polarimetry, the required minimum measurements for deducing Stokes vectors are 4. The EWV value for those temporal phases at 0, 30, 90, and 210° is 5, which is about one-quarter of the value for the classical rotating retarder and fixed polarizer system (RRFP) technique, as shown in **Figure 7**. Compared with the EWV value of the RRFP system under various configurations, one can observe that the noise is considerably reduced under the optimized phase retardation condition, but the angular positions have very limited effect on their EWV value. Since the EWV value can be used to quantitatively evaluate the noise immunity of a polarimetry, we can conclude that if one wants to achieve the same signal-to-noise ratio for 4 temporal phase measurements in the PEM polarimetry, one needs 8 measurements in the optimal orientations under optimal retardation and more than 16 uniformly spaced measurements over 360° in the RRFP configuration with quarter-wave retardation.

3.4. PEM imaging ellipsometric measurement with the dual-wavelength approach

In the previous section, two-dimensional ellipsometric parameters were determined at a specific wavelength. In the conventional PEM-based ellipsometric measurement, the modulation
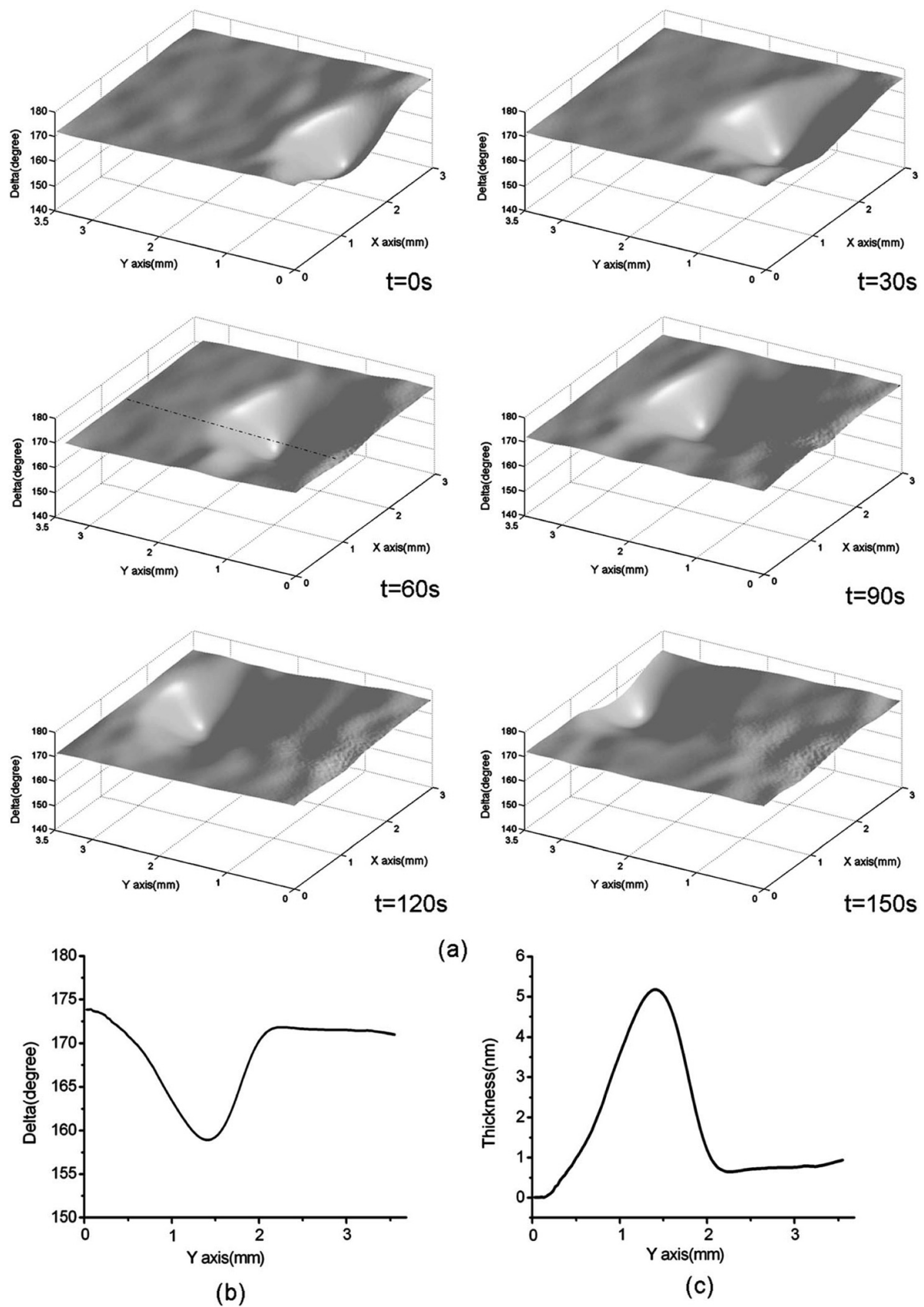
Figure 5. The movement behavior of an oil droplet: (a) Δ distribution for every 30 s, (b) the cross-sectional distribution of Δ through the center of the oil droplet at t = 60 s, and (c) the thickness profile across the center of the oil droplet at t = 60 s.
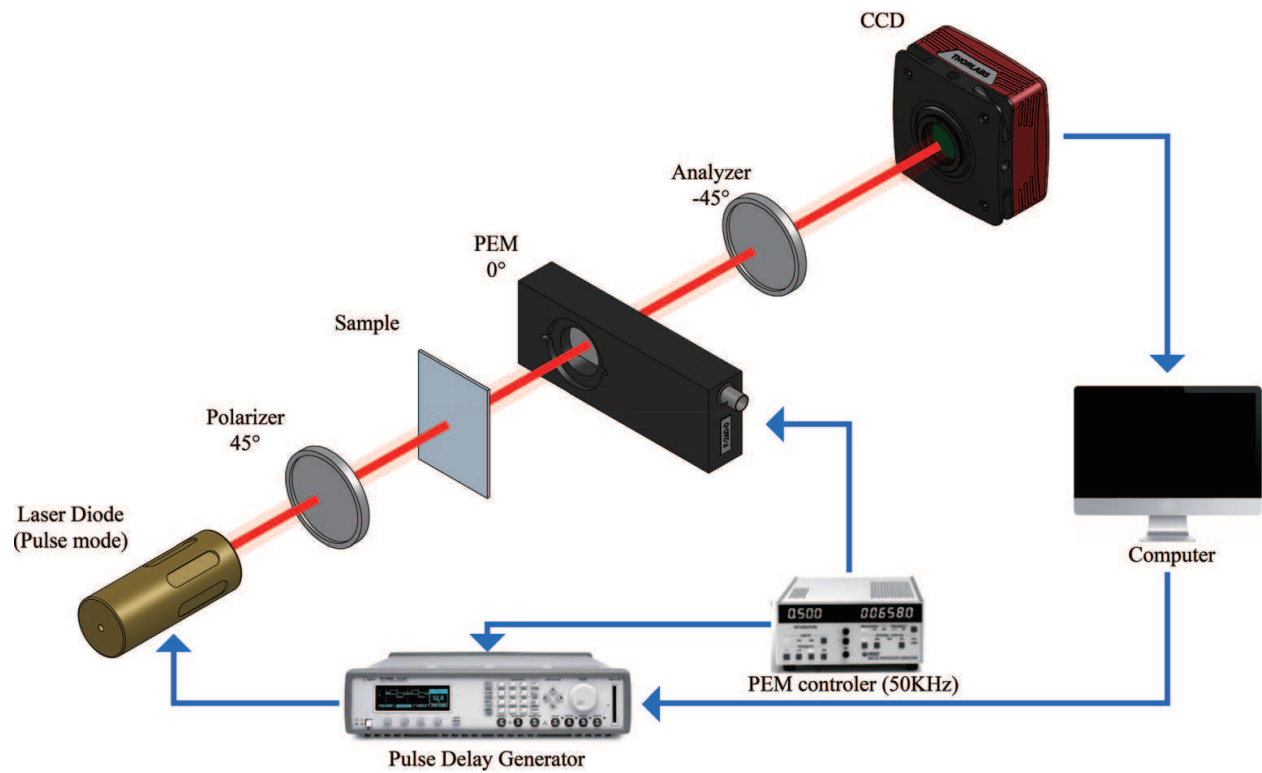
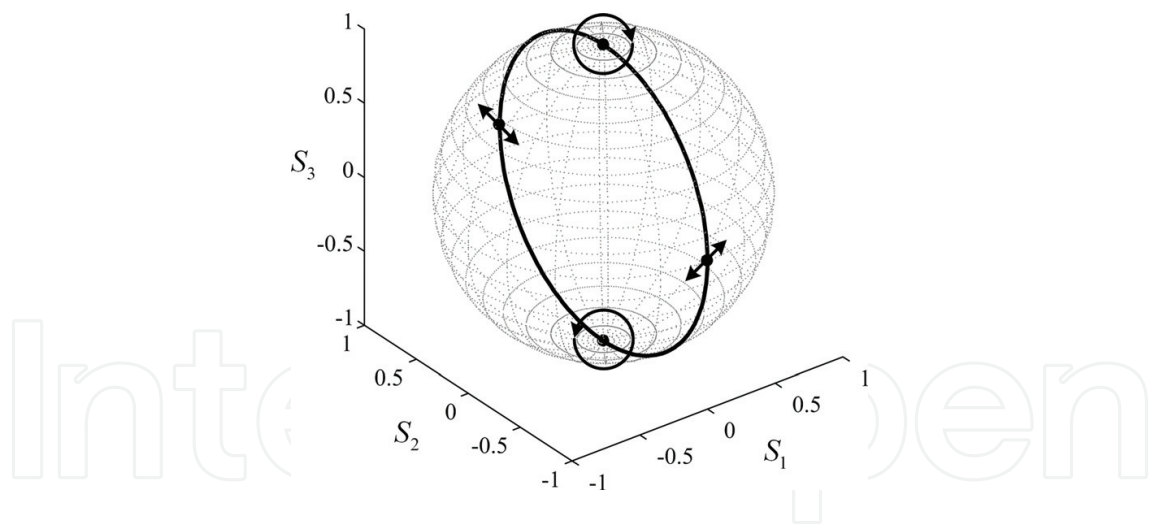**Figure 6.** System configuration of the phase-lock PEM polarimetry for Stokes parameters measurement.

Figure 7. Trajectory of the phase-lock PEM polarimetry on the Poincar'e sphere: the four specific polarization states are indicated in the graph.

amplitude is controlled by applying an external voltage for a specific wavelength. However, a few seconds are required to reach resonance equilibrium and stabilize the modulator, while there is a change in the modulation amplitude for different wavelength; this procedure significantly reduced the measurement speed for the multi-wavelength measurement. Here, we developed an equivalent phase retardation technique that may help prevent the above disadvantage of PEM for multi-wavelength measurement [17]. In general, the half-wave modulation

is set at a specific wavelength (λ_1). However, while the wavelength of the incident light shifts to the other shorter wavelength (λ_2), the modulation amplitude no longer equals 0.5 waves, but rather equals $0.5/\lambda_2$ waves. We changed the temporal phase angle ωt to maintain a constant dynamic retardation of the PEM, rather than the applied voltage, while the original wavelength λ_1 switches to the other λ_2. Their relation is as follows:

$$\Delta_p = \frac{0.5\lambda_1}{\lambda_2} \sin \omega t \qquad (23)$$

According to the Eq. (22), **Figure 8** demonstrates that though the wavelength was changed from one to the other, the output polarizations were kept constant by setting different temporal phase angles within a modulation cycle. **Figure 9** shows the thickness profile of a two-step oxidized silicon wafer examined using red and blue light, respectively. **Table 1** lists the measured ellipsometric parameters and deduced film thickness from both wavelengths. To sum up, the film thicknesses measured were close to the theory whether by red or blue lights.

3.5. Full Mueller matrix imaging polarimetry based on the hybrid phase modulation

Mueller matrix imaging contains comprehensive information on the morphological and functional properties of the biological samples as well as the birefringence, dichroism, and depolarization of the specimens [31–33]. The conventional Mueller matrix imaging approaches were based on measurements involving sequential rotation of the polarizer, analyzer, and retarders,
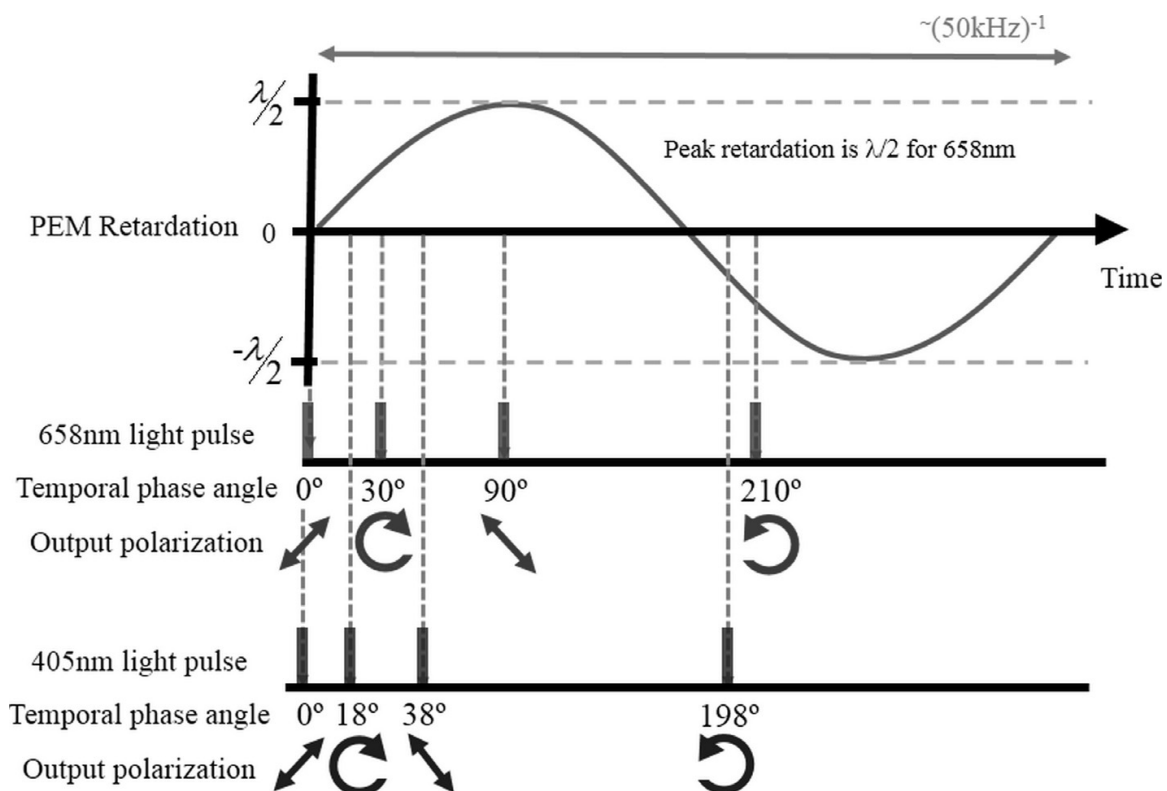

Figure 8. Polarization modulation at peak retardation of half-wave (λ = 658 nm) and the output polarization at four temporal phase angles of dual-wavelength.
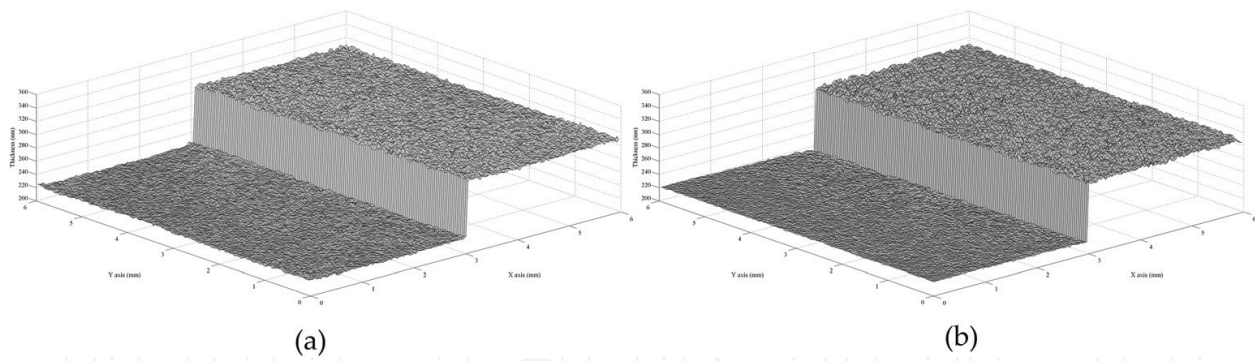
(a)
(b)

Figure 9. Oxide thickness profile of the two-step reference wafer. (a) the deduced thickness profile by 658 nm red light source and (b) the deduced thickness profile by 405 nm blue light source.

Wavelength (nm)	Index of refraction	Measured ellipsometric parameters		Deduced film thickness (nm)
		$\Delta(°)$	$\Psi(°)$	
658	Si:3.836-i0.016 SiO$_2$:1.456	166.03 ± 1.12	11.69 ± 0.08	5.20 ± 0.43
405	Si:5.424-i0.330 SiO$_2$:1.469	159.72 ± 1.36	22.58 ± 0.38	5.57 ± 0.45

Table 1. Optical characteristics for the substrate and thin films.

but such approach was a time-consuming process that impeded the use of the system for in vivo imaging studies. In order to improve the speed of measurement, recent development in the Mueller matrix polarimeter was mainly focused on the process of using liquid crystal to control and analyze the state of the input or output polarizations. As the measurements with these approaches usually employed unmodulated light irradiance, the results were more sensitive to noise than methods using an intensity modulated light, particularly for highly scattering samples [34, 35]. Moreover, the tuning curve of the liquid crystal variable redarder (LCVR) was found to be sensitive to its alignment and temperature to result in systematic errors and also impact the overall performance of the instrument [36].

The deficiency of LCVRs in the Mueller matrix imaging system can be improved by replacing the LCVRs in the portion of the polarization state analyzer with a PEM, and the modified configuration is shown in **Figure 10** [18]. The polarization state generator of this system is composed of a linear polarizer and two LCVRs. The azimuth angle of the polarizer was set at $-45°$ and the slow axis of the two LCVRs was oriented to an angle of 90 and $45°$, respectively. The retardations (δ_1, δ_2) of both LCVRs are dependent on their driving voltages to generate four polarizations. Thus, the Mueller matrix of the PSG in terms of the Mueller matrices of their components can be expressed as:

$$M_{PSG} = M_{LCVR_2}(\delta_2, 45°) \bullet M_{LCVR_1}(\delta_1, 90°) \bullet M_P(-45°) \tag{24}$$

The polarization state analyzer (PSA) was composed of a PEM and an analyzer. In order to obtain a complete set of PSA, we set the azimuth angle of the PEM at $0°$, and the Mueller matrix representing the PSA module is obtained from:
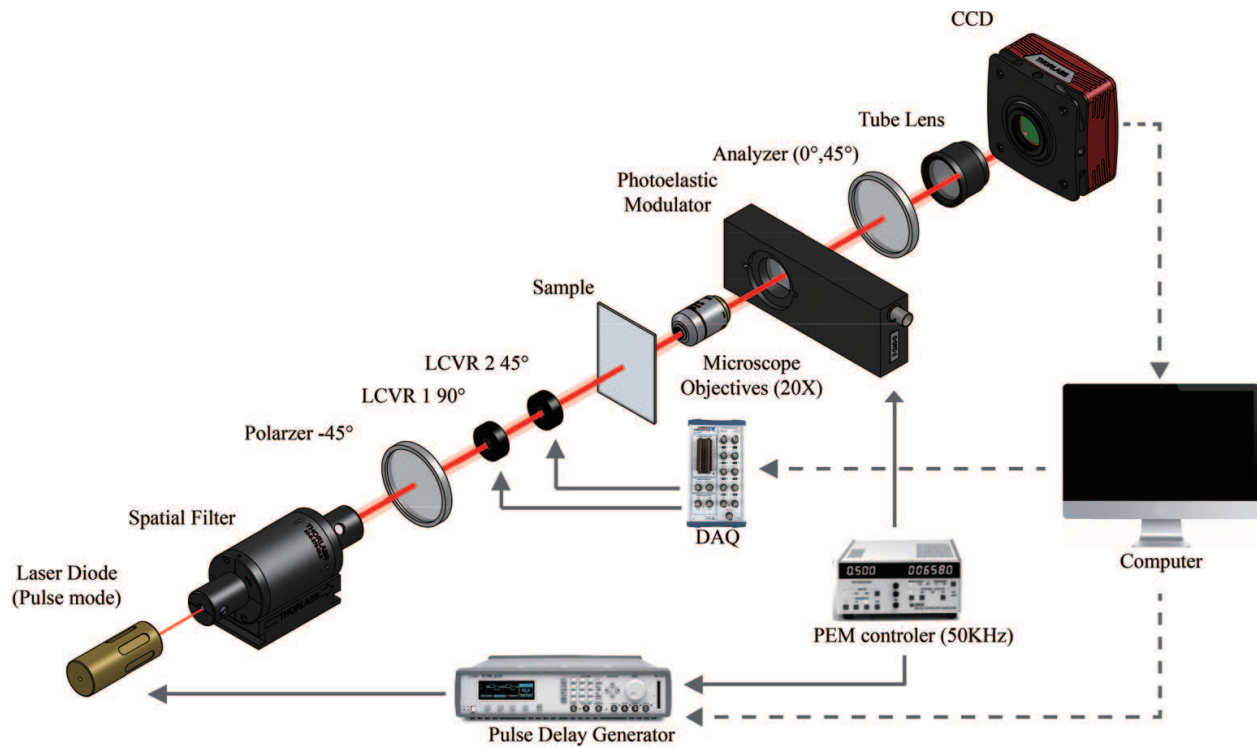
Figure 10. Optical setup for Mueller matrix imaging polarimetry with hybrid phase modulation technique.

$$M_{PSA} = M_A(A) \bullet M_{PEM}(\Delta_p, 0°) \tag{25}$$

where M_A and M_{PEM} are the Mueller matrix of the analyzer and PEM, respectively; A is the azimuth angle of the analyzer; and Δ_p represents the phase retardation of the PEM, which was also modulated as $\delta_0 \sin \omega p$. Here, the amplitude of modulation δ_0 is set at π, and the temporal phase angle refers to Δ_p. Consequently, the total Mueller matrix of the system is given by:

$$M_T = M_{PSA} M_S M_{PSG} = M_a(A) \bullet M_{PEM}(\Delta_p, 0°) \bullet M_S \bullet M_{LCVR_2}(\delta_2, 45°) \bullet M_{LCVR_1}(\delta_2, 90°) \bullet M_P(-45°) \tag{26}$$

where M_S is represented as the Mueller matrix of the sample being tested. As the system is based on intensity modulation, only the first element of the Stokes parameters in Eq. (25) has to be considered. One can formulate the temporal intensity behavior as follows:

$$
\begin{aligned}
I(A, \theta_p, \delta_1, \delta_2) = \frac{I_0}{4} \langle & m_{00} - m_{02} \cos \delta_1 - \frac{1}{2} m_{01} \sin \delta_1 \sin \delta_2 \\
& + \cos 2A \left(m_{10} - \frac{1}{2} m_{11} \sin \delta_1 \sin \delta_2 - m_{12} \cos \delta_1 + m_{13} \sin \delta_1 \cos \delta_2 \right) \\
& + \frac{1}{2} \sin 2A [\cos(\pi \sin \theta_p)(2 m_{20} - m_{21} \sin \delta_1 \sin \delta_2 - 2 m_{22} \cos \delta_1) \\
& + \sin(\pi \sin \theta_p)(2 m_{30} \sin 2A - m_{31} \sin \delta_1 \sin \delta_2 - 2 m_{32} \sin 2A)] \\
& + \sin \delta_1 \cos \delta_2 \{ m_{03} + \sin 2A [m_{23} \cos(\pi \sin \theta_p) + m_{33} \sin(\pi \sin \theta_p)]\} \rangle
\end{aligned}
\tag{27}
$$

It is well-known principles that at least 16 individual polarization state measurements are required to determine the full Mueller matrix. The measurements are usually carried out by generating four specific polarization states from the PSG, and each output polarization can be determined by at least four intensity measurements. Accordingly, both the PSG and the PSA must be "complete" to obtain the full Mueller matrix with at least four basic states.

In detail, the four phase retardations $(\delta_1, \delta_2) = (90°, 0°), (0°, 0°), (75.5°, 206.5°),$ and $(75.5°, 153.5°)$ were sequentially set for both LCVRs, so that four specific polarization states were generated from the PSG. In order to characterize the Stokes vectors of the outgoing light from the sample, four conditions were also set up for the PSA by changing the azimuth of the analyzer A and the temporal phase angle Δ_p of the PEM, with the following conditions: $(A, \Delta_p) = (0°, 0), (45°, 0°), (45°, 30°),$ and $(45°, 90°)$. While capturing the images with different conditions of the PSG and the PSA, the modulated pulse is achieved by a DC bias current equal to the threshold value coupled with a programmable pulse generator to drive the laser diode. The generated and analyzed polarization states, in the order of the optimal optical settings, and the exact 16 intensity measurements were obtained as shown in **Table 2**, while the details for determining individual Mueller matrix elements are listed in **Table 3**.

Two results were shown by using this Mueller matrix imaging measurement system. The first results were the measured Mueller matrices of a quarter wave plate and the map of its phase retardation. We set the azimuth angle of the wave plate at $0°$, which makes $m_{23} = 1, m_{32} = -1, m_{22} = 0,$ and $m_{33} = 0$; the values of other elements were the same as those in air. Also, we rotated the quarter wave plate to set its azimuth angle at 30 and $60°$ and deduced its phase retardation by the Lu-Chipman algorithm, as shown in **Figure 11**. The average value of the phase retardation, which is close to the ideal condition at around $90°$, and the azimuth angle under different rotation conditions are shown in **Figure 12**. Disregarding some static areas with small deviations due to speckles of dust in the imaging elements, the measured distributions almost matched the theoretical conditions.

The other result was the dynamic optical characteristics of a biopolymer specimen with heat-induced conformational change. The second test sample, shrimp shell, is composed of chitin, proteins, lipids, and pigments and with the characteristic of being semi-transparent. Accordingly, we investigated the conformational changes of shrimp shell induced by heat treatment,

PSG (δ_1, δ_2)	PSA (Analyzer, PEM)			
	$(0°, 0°)$	$(45°, 0°)$	$(45°, 30°)$	$(45°, 90°)$
$(75.5°, 206.5°)$	I_4	I_5	I_6	I_7
$(75.5°, 153.5°)$	I_3	I_{10}	I_9	I_8
$(0°, 0°)$	I_2	I_{11}	I_{12}	I_{13}
$(90°, 0°)$	I_1	I_{16}	I_{15}	I_{14}

Table 2. Measurement sequence of 16 intensities under the condition of retardation of LCVRs for the chosen set of analyzer and temporal phase angle of the PEM.

Element	Intensity calculation
m_{00}	$\left(2 \cdot \left(2I_{10} - I_{11} - I_{13} + 2I_5 + 2I_7 + 2I_8 + 2\sqrt{3}(I_{14} + I_{16})\right)\right)/(2\sqrt{3} + 3)$
m_{01}	$4\sqrt{3} \cdot (I_{10} - I_5 - I_7 + I_8)$
m_{02}	$\left(4 \cdot \left(I_{10} - 2I_{11} - 2I_{13} + I_5 + I_7 + I_8 - \sqrt{3}(I_{11} + I_{13} - I_{14} - I_{16})\right)\right)/(2\sqrt{3} + 3)$
m_{03}	$\left(2 \cdot (2I_{10} - I_{11} - I_{13} - 3I_{14} - 3I_{16} + 2I_5 + 2I_7 + 2I_8)\right)/(2\sqrt{3} + 3)$
m_{10}	$-\left(2 \cdot \left(2I_{10} - I_{11} - I_{13} + 2I_2 - 4I_3 - 4I_4 + 2I_5 + 2I_7 + 2I_8 - 4\sqrt{3}I_1 + 2\sqrt{3}(I_{14} + I_{16})\right)\right)/(2\sqrt{3} + 3)$
m_{11}	$4\sqrt{3} \cdot (I_{10} - 2I_2 + 2I_4 - I_5 - I_7 + I_8)$
m_{12}	$-\left(4 \cdot \left(I_{10} - 2I_{11} - 2I_{13} + 4I_2 - 2I_3 - 2I_4 + I_5 + I_7 + I_8 - 2\sqrt{3}(I_1 - I_2) - \sqrt{3}(I_{11} + I_{13} - I_{14} - I_{16})\right)\right)/(2\sqrt{3} + 3)$
m_{13}	$-\left(2 \cdot (6I_1 + 2I_{10} - I_{11} - I_{13} - 3I_{14} - 3I_{16} + 2I_2 - 4I_3 + 2I_5 + 2I_7 + 2I_8)\right)/(2\sqrt{3} + 3)$
m_{20}	$\left(2 \cdot \left(2I_{10} - I_{11} + I_{13} + 2I_5 - 2I_7 - 2I_8 - 2\sqrt{3}(I_{14} + I_{16})\right)\right)/(2\sqrt{3} + 3)$
m_{21}	$4\sqrt{3} \cdot (I_{10} - I_5 + I_7 - I_8)$
m_{22}	$\left(4 \cdot \left(I_{10} - 2I_{11} + 2I_{13} + I_5 - I_7 - I_8 - \sqrt{3}(I_{11} - I_{13} + I_{14} - I_{16})\right)\right)/(2\sqrt{3} + 3)$
m_{23}	$\left(2 \cdot (2I_{10} - I_{11} + I_{13} + 3I_{14} - 3I_{16} + 2I_5 - 2I_7 - 2I_8)\right)/(2\sqrt{3} + 3)$
m_{30}	$-\left(2 \cdot \left(2I_{10} - I_{11} + 2I_{12} - I_{13} + 2I_5 - 4I_6 + 2I_7 + 2I_8 - 4I_9 - 4\sqrt{3}I_{15} + 2\sqrt{3}(I_{14} + I_{16})\right)\right)/(2\sqrt{3} + 3)$
m_{31}	$4\sqrt{3} \cdot (I_{10} - I_5 + 2I_6 - I_7 + I_8 - 2I_9)$
m_{32}	$-\left(4 \cdot \left(I_{10} - 2I_{11} - 2I_{13} + 4I_{12} + I_5 - 2I_6 + I_7 + I_8 - 2I_9 - 2\sqrt{3}(I_{15} - I_{12}) - \sqrt{3}(I_{11} + I_{13} - I_{14} - I_{16})\right)\right)/(2\sqrt{3} + 3)$
m_{33}	$-\left(2 \cdot (2I_{10} - I_{11} + 2I_{12} - I_{13} - 3I_{14} + 6I_{15} - 3I_{16} + 2I_5 - 4I_6 + 2I_7 + 2I_8 - 4I_9)\right)/(2\sqrt{3} + 3)$

Table 3. Set of 16 intensities for calculating the full Mueller matrix elements.
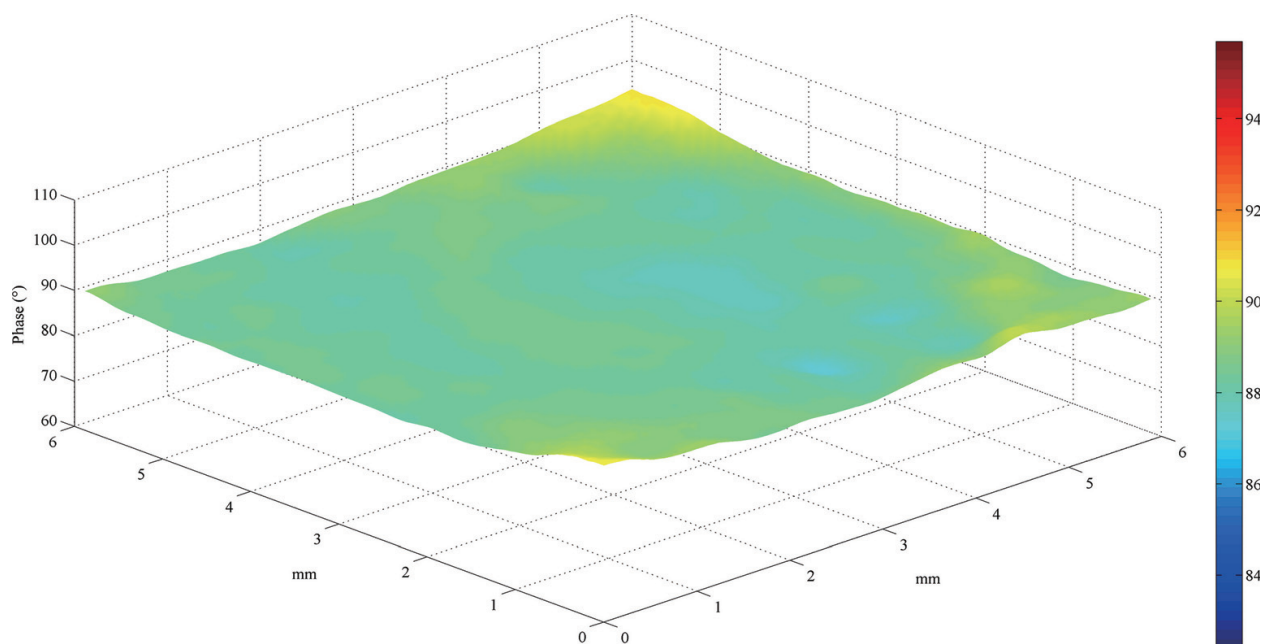

Figure 11. Phase distribution of the measured quarter wave plate while the azimuth angle was set at $0°$.
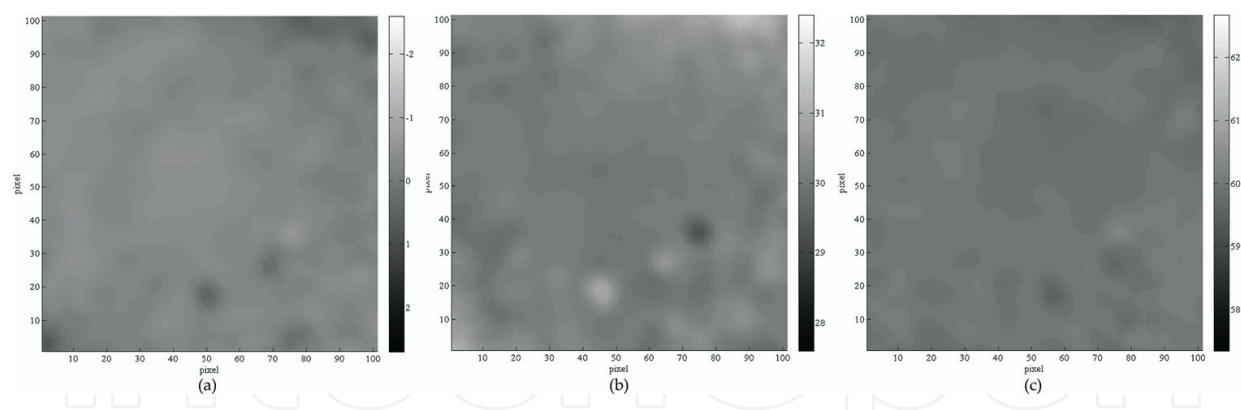
Figure 12. Azimuth angle distribution of the measured quarter wave plate while the azimuth angle was set at (a) 0°, (b) 30°, and (c) 60°.

because shrimp shell is a birefringent biopolymer material, whose absorption spectrum and transparency could be changed during the heat treatment. Therefore, the optical characteristics, such as diattenuation, depolarization, and phase retardation of the shrimp shell may be changed by heat treatment. During the examination, the shrimp shell was heated by a thermal electrical source to make it gradually turn to ruby red with the increase of the temperature. Meanwhile, a set of 16 images were recorded every 90 seconds to deduce the full elements of the Mueller matrix images. The retrieved polarization parameters, including retardance (R), depolarization coefficient (Δ), and diattenuation (d) deduced by the Lu-Chipman algorithm are shown in **Table 4**. Since the value of R was mainly related to the change of thickness or structure of the sample, the average value of R around 50° before and after the heat treatment of the shrimp shell represents thickness or structure that remained unchanged. Since the heat

Table 4. Decomposed experimental Mueller matrix images of the shrimp shell by heating treatment.

source was located below the sample, the depolarization coefficient (Δ) appeared as the bottom-up change specification. One can observe that the overall trends for depolarization and diattenuation share common features due to heat treatment that induces the crustacean to relax its bonds with astaxanthin, which causes the shell to be transformed from almost transparent to red. In this process, the binding of both proteins would increase the scattering effect of the incident light. However, the behavior of the protein complex and transformation of the polarization properties associated with the Mueller matrix needs further exploration.

4. Conclusions

The known commercial imaging ellipsometry, usually employing the zone-averaging approach, is in the order of minutes to obtain two-dimensional optical characteristics of a thin film. In this chapter, we demonstrate the stroboscopic illumination technique in PEM-based ellipsometry just by using a limited number of measurements that can reduce the acquisition time in imaging ellipsometry and carry out the measurement within a few seconds. In addition to making use of this technique for imaging ellipsometry measurement, this approach was also extended to Stokes parameters and Mueller matrix imaging. Under the condition of multi-wavelength or spectroscopic measurement, polarimetry usually encounters the issue of retardation dispersion, which is the same situation that one encounters while using the PEM in an ellipsometry system. We developed the equivalent phase retardation technique, in which retardation dispersion settings of the PEM for different wavelengths were not required. That is to say, the stability and frame rate for the multi-wavelength measurement were almost the same as the single wavelength approach. The ellipsometric parameters of different wavelengths were capable of determining additional sample parameters, such as surface roughness, multiple film thicknesses, index dispersion, and the consistency of deduced results. Since polarization behavior of transmitted or reflected light was strongly related to their wavelength, multi-wavelength approach for Stokes parameters and Mueller matrix imaging can enhance the contrasts and increase the sensitivity of measurements for some features of the biological samples. If the polarimetry system can quickly obtain the desired images, we believe polarimetry imaging is well placed for in vivo tissue diagnosis in the forthcoming future [24].

Author details

Chien-Yuan Han[1]*, Yu-Faye Chao[2] and Hsiu-Ming Tsai[3]

*Address all correspondence to: cyhan@gm.nuu.edu.tw

1 Department of Electro-Optical Engineering, National United University, Miaoli, Taiwan (ROC)

2 Department of Photonics, National Chiao Tung University, Hsinchu, Taiwan(ROC)

3 Department of Radiology, The University of Chicago, Chicago, USA

References

[1] Tompkins HG. Industrial applications of spectroscopic ellipsometry. Thin Solid Films. 2004;**455–456**:772-778. DOI: 10.1016/j.tsf.2004.01.045

[2] Jin G, Meng YH, Liu L, Niu Y, Chen S, Cai Q, et al. Development of biosensor based on imaging ellipsometry and biomedical applications. Thin Solid Films. Amsterdam and New York, 2011;**519**:2750-2757. DOI: 10.1016/j.tsf.2010.12.175

[3] Fukuzawa K, Shimuta T, Nakada A, Zhang H, Mitsuya Y. Measurement of thickness of molecularly thin lubricant film using ellipsometric microscopy. IEEE Transactions on Magnetics. 2005;**41**:808-811. DOI: 10.1109/TMAG.2004.840349

[4] Azzam RMA, Bashara NM. Ellipsometry and Polarized Light. North Holland Publishing Co; 1978. p. 270-271. DOI: 10.1063/1.2994821

[5] Drévillon B. Phase modulated ellipsometry from the ultraviolet to the infrared: In situ application to the growth of semiconductors. Progress in Crystal Growth and Characterization of Materials. 1993;**27**:1-87. DOI: 10.1016/0960-8974(93)90021-U

[6] Asinovski L, Beaglehole D, Clarkson MT. Imaging ellipsometry: Quantitative analysis. Applications and Materials Science. 2008;**771**:764-771. DOI: 10.1002/pssa.200777855

[7] Qingqing L, Fukuzawa K, Kajihara Y, Zhang H, Itoh S. Development of ellipsometric microscope for high-resolution observation of nanometer-thick lubricant films. Tribology Online. 2011;**6**:251-256. DOI: 10.2474/trol.6.251

[8] Noort DV, Rumberg J, Jager EWH, Mandenius CF. Silicon based affinity biochips viewed with imaging ellipsometry. Measurement Science and Technology. 2000;**11**:801-808. DOI: 10.1088/0957-0233/11/6/325

[9] Chao YF, Lee KY. Index profile of radial gradient index lens measured by imaging ellipsometric technique. Japanese Journal of Applied Physics. 2005;**44**:1111-1114. DOI: 10.1143/JJAP.44.1111

[10] Han CY, Lee ZY, Chao YF. Determining thickness of films on a curved substrate by use of ellipsometric measurements. Applied Optics. 2009;**48**:3139-3143. DOI: 10.1364/AO.48.003139

[11] Graf RT, Eng F, Koenig JL, Ishida H. Polarization modulation fourier transform infrared ellipsometry of thin polymer films. Applied Spectroscopy. 1986;**40**:498-503. DOI: 10.1366/0003702864508818

[12] Vallon S, Compain E, Drévillon B. Improvements of fourier transform phase-modulated ellipsometry. Review of Scientific Instruments. 1995;**66**:3269-3272. DOI: 10.1063/1.1145492

[13] Khazimullin MV, Lebedev YA. Fourier transform approach in modulation technique of experimental measurements. Review of Scientific Instrumens. 2010;**81**:043110. DOI: 10.1063/1.3327844

[14] Han CY, Chao YF. Photoelastic modulated imaging ellipsometry by stroboscopic illumination technique. Review of Scientific Instruments. 2006;**77**:023107. DOI: 10.1063/1.2173027

[15] Tsai HM, Chen CW, Tsai TH, Chao YF. Deassociate the initial temporal phase deviation provided by photoelastic modulator for stroboscopic illumination polarization modulated ellipsometry. Review of Scientific Instruments. 2011;**82**:035117. DOI: 10.1063/1.3568745

[16] Tsai HM, Chao YF. Optimization of a four-temporal phase lock for photoelastic-modulated polarimetry. Optics Letter. 2009;**34**:2279-2281. DOI: 10.1364/OL.34.002279

[17] Kuo CW, Han CY, Jhou JY, Peng ZY. Using a fast dual-wavelength imaging ellipsometric system to measure the flow thickness profile of an oil thin film. Applied Surface Science. http://www.sciencedirect.com/science/article/pii/S0169433217301010. DOI: 10.1016/j.apsusc.2017.01.100

[18] Han CY, Du CY, Jhou JY. Rapid full Mueller matrix imaging polarimetry based on the hybrid phase modulation technique. Optics Communication. 2017;**382**:501-508. DOI: 10.1016/j.optcom.2016.08.026

[19] Wang B, List J. Basic optical properties of the photoelastic modulator: Part I. Useful aperture and acceptance angle. Proceedins of SPIE. 2005;**5888**:58881I. DOI: 10.1117/12.617904

[20] Wang B, Hinds E, Krivoy E. Basic optical properties of the photoelastic modulator part II: Residual birefringence in the optical element. Proceedings of SPIE. 2009;**7461**:746110. DOI:10.1117/12.826392

[21] Zeng A, Li F, Zhu L, Huang H. Simultaneous measurement of retardance and fast axis angle of a quarter-wave plate using one photoelastic modulator. Applied Optics. 2011;**50**:4347-4352. DOI: 10.1364/AO.50.004347

[22] Gribble A, Layden D, Vitkin IA. Experimental validation of optimum input polarization states for Mueller matrix determination with a dual photoelastic modulator polarimeter. Optics Letters. 2013;**38**:5272-5275. DOI: 10.1364/OL.38.005272

[23] Alali S, Yang T, Vitkin IA. Rapid time-gated polarimetric Stokes imaging using photoelastic modulators. Optics Letters. 2013;**38**:2997-3000. DOI: 10.1364/OL.38.002997

[24] Alali S, Vitkin A. Polarized light imaging in biomedicine: Emerging Mueller matrix methodologies for bulk tissue assessment. Journal of Biomedical Optics. 2015;**20**:61104. DOI: 10.1117/1.JBO.20.6.061104

[25] Alali S, Gribble A, Vitkin IA. Rapid wide-field Mueller matrix polarimetry imaging based on four photoelastic modulators with no moving parts. Opt Lett.2016;**41**:1038–1041. DOI: 10.1364/OL.41.001038

[26] Wang M, Chao Y, Wang M, Chao Y, Leou K, Chao YF, et al. A direct determination technique for Azimuth alignment in photoelastic modulation ellipsometry. Japanese Journal of Applied Physics. 1999;**38**:6919-6922. DOI: 10.1143/JJAP.38.6919

[27] Wang MW, Chao YF. Azimuth alignment in photoelastic modulation ellipsometry at a fixed incident angle. Japanese Journal of Applied Physics. 2002;**41**:3981-3986. DOI: 10.1143/JJAP.41.3981

[28] Wang MW, Chao YF, Leou KC, Tsai FH, Lin TL, Chen SS, et al. Calibrations of phase modulation amplitude of photoelastic modulator. Japanese Journal of Applied Physics. 2004;**43**:827-832. DOI: 10.1143/JJAP.43.827

[29] Collett E. Polarized Light: Fundamentals and Applications. New York: Marcel Dekker; 1993. p. 581

[30] Sabatke DS, Descour MR, Dereniak EL, Sweatt WC, Kemme SA, Phipps GS. Optimization of retardance for a complete Stokes polarimeter. Optics Letters. 2000;**25**:802-804. DOI: 10.1364/OL.25.000802

[31] Chen C, An I, Ferreira GM, Podraza NJ, Zapien JA, Collins RW. Multichannel Mueller matrix ellipsometer based on the dual rotating compensator principle. Thin Solid Films. 2004;**455–456**:14-23. DOI: 10.1016/j.tsf.2003.11.191

[32] Dubreuil M, Rivet S, LeJeune B, Cariou J. Snapshot Mueller matrix polarimeter by wavelength polarization coding. Optics Express. 2007;**15**:13660-13668. DOI: 10.1364/OE.15.013660

[33] Gao M, Yang P, Mckee D, Kattawar GW. Mueller matrix holographic method for small particle characterization: Theory and numerical studies. Applied Optics. 2013;**52**:5289-5296. DOI: 10.1364/AO.52.005289

[34] Laude Boulesteix B, De Martino A, Drévillon B, Schwartz L. Mueller polarimetric imaging system with liquid crystals. Applied Optics. 2004;**43**:2824-2832. DOI: 10.1364/AO.43.002824

[35] De Martino A, Kim YK, Garcia Caurel E, Laude B, Drévillon B. Optimized Mueller polarimeter with liquid crystals. Optics Letters. 2003;**28**:616-618. DOI: 10.1364/OL.28.000616

[36] Babilotte P, Nunes Henrique Silva V, Sathaye K, Dubreuil M, Rivet S, Dupont L, et al. Twisted ferroelectric liquid crystals dynamic behaviour modification under electric field: A Mueller matrix polarimetry approach using birefringence. Japanese Journal of Applied Physics. 2014;**115**:34906. DOI: 10.1063/1.4862162